HIGH POWER CO LASER

G. L. McAllister, et al

Northrop Research and Technology Center

Prepared for:

Office of Naval Research
Advanced Research Projects Agency

May 1974

HIGH POWER CO LASER
SEMIANNUAL TECHNICAL REPORT

Period Covering:
September 1, 1973 - February 28, 1974

May 1974

Prepared by

Northrop Research and Technology Center
G. L. McAllister, W. B. Lacina
D. K. Rice, P. J. Mendoza

Contract N00014-72-C-0043

Sponsored by
ADVANCED RESEARCH PROJECTS AGENCY
ARPA ORDER NO. 1807

Monitored by
OFFICE OF NAVAL RESEARCH
CODE 421

NORTHROP CORPORATION
Northrop Research and Technology Center
Laser Technology Laboratories
3401 West Broadway
Hawthorne, California 90250

PROGRAM IDENTIFICATION

ARPA Order No.:	1807
Program Code No.:	3E90
Name of Contractor:	Northrop Corporation
Effective Date of Contract:	1 August 1971 - 30 June 1974
Amount of Contract:	$3,533,763
Contract No.:	N00014-72-C-0043
Program Manager:	Dr. G. L. McAllister (213) 675-4611, Ext. 4975
Scientific Officer:	Director, Physics Program Physical Sciences Division Office of Naval Research Department of the Navy 800 North Quincy Arlington, Virginia 22217

Disclaimer: The views and conclusions contained in this document are those of the authors and should not be interpreted as necessarily representing the official policies, either expressed or implied, of the Advanced Research Projects Agency or the U. S. Government.

TABLE OF CONTENTS

1.0	SUMMARY		1
2.0	LINE SELECTION		4
	2.1	Absorption Cell Assembly	4
	2.2	Absorption Cell Oven	4
	2.3	Absorption Cell System	7
	2.4	Calibration and Testing of Absorption Cell System	7
	2.5	Optical Quality Investigations	9
3.0	A NOMINAL 10-LITER LASER SYSTEM		19
	3.1	Experimental Investigations with CO/Argon Gas Mixtures	19
	3.2	Effects of Electron Beam Scattering	21
	3.3	Laser Medium Interferometry	28
REFERENCES			36

1.0 SUMMARY

The long range objective of this program is to develop the necessary technology for a high average power, repetitively pulsed, diffraction limited CO laser operating at an electrical efficiency of 50% or more. The work covered in this contract involves the design of intermediate power CO laser devices, the development of the required CO laser technology, and the construction and testing of an intermediate energy CO laser device.

This program encompasses, on a best effort basis, the following major tasks:

1. The development of both steady state and transient kinetic models in order that realistic theoretical predictions of high energy device characteristics can be made.

2. Measurements of basic parameters of the CO laser at low pressures including: gain, saturation intensity, rates of vibrational cross-relaxation between CO molecules, transfer rates of CO and N_2, discharge characteristics, and spectral characteristics.

3. Measurements and characterization of a high pressure E-beam excited pulsed laser to experimentally determine transient operating parameters for high energy extraction.

4. The design and construction of a 500J/pulse diffraction-limited CO laser oscillator.

5. The development of line selection techniques for controlling the oscillator spectral output.

During this period the water vapor cell and oven assembly were tested separately from the laser both mechanically and optically. This device will be installed in the 10-liter laser to achieve rotational line selection, restricting the laser emission to only those lines which are transmitted through the atmosphere. The system was operated at pressures up to 3 atmospheres and temperatures up to 175°C with no leaks and no condensation of water vapor. A Mach-Zehnder interferometer was used to analyze the optical quality of the system under operating conditions. The only significant optical distortion was the infrequent occurrence of thermal risers in the cell. It is concluded from these studies that the system is ready for installation in the device.

Investigation with the 10-liter E-beam CO laser continued during this period. Parametric measurements were made with Ar/CO gas mixtures and the results compared to the CO laser kinetics code projections. The electrical excitation energy required to reach laser threshold was measured to be approximately 0.6 J/ℓ-torr over the pressure range from 80 to 140 torr. This value is in good agreement with the scaling generalizations derived from the kinetics code. The excitation required to reach steady-state was measured to be approximately 2.0 J/ℓ-torr which is also in good agreement with the scaling generalizations.

The effect of electron beam scattering was investigated by observing near-field burn patterns as the electron accelerating voltage was changed and as the laser gas pressure was changed. Reducing the accelerating voltage from 175 kV to 150 kV caused a noticeable deterioration and increasing the argon pressure from 75 torr to 150 torr caused a dramatic effect. As the scattering is increased either by reducing the voltage or by increasing the gas pressure the electrical excitation rate increases near the anode resulting in a near-field pattern which is much more intense in this region. Theoretical scattering calculations were used in conjunction

with the theoretical results from the kinetics code to estimate the non-uniformity caused by this problem. It is concluded that argon pressures much higher than 150 torr will not be useful in the present configuration.

A pulsed ruby laser interferometer was used in both a single pulse mode and double pulse mode to study the optical quality of the laser gas medium. Double pulse interferograms have shown that the stability of the entire system including the cryogenic laser gas and the interferometer is better than $\lambda/2$ at 5 μm over time intervals up to and in excess of two minutes. Single pulse interferograms taken with electrical excitation but without optical extraction clearly show the acoustical disturbances produced by the intense heating in the cathode fall region and by the bulk heating of the laser gas. Analysis of these results is in progress and should lead to values for the cathode fall and bulk heating rates.

UNCLASSIFIED

SECURITY CLASSIFICATION OF THIS PAGE *(When Data Entered)*

REPORT DOCUMENTATION PAGE		READ INSTRUCTIONS BEFORE COMPLETING FORM
1. REPORT NUMBER NRTC 74-21R	2. GOVT ACCESSION NO.	3. RECIPIENT'S CATALOG NUMBER AD-780265
4. TITLE *(and Subtitle)* High Power CO Laser Semiannual Technical Report - Period Covering: September 1, 1973 - February 28, 1974		5. TYPE OF REPORT & PERIOD COVERED Semiannual Technical Report 6. PERFORMING ORG. REPORT NUMBER
7. AUTHOR(s) G. L. McAllister, W. B. Lacina, D. K. Rice, P. J. Mendoza		8. CONTRACT OR GRANT NUMBER(s) -C- N00014-72-0043
9. PERFORMING ORGANIZATION NAME AND ADDRESS Northrop Research and Technology Center 3401 West Broadway Hawthorne, California 90250		10. PROGRAM ELEMENT, PROJECT, TASK AREA & WORK UNIT NUMBERS ARPA Order No. 1806
11. CONTROLLING OFFICE NAME AND ADDRESS Advanced Research Projects Agency 1400 Wilson Blvd. Arlington, Virginia		12. REPORT DATE May 1974 13. NUMBER OF PAGES 37
14. MONITORING AGENCY NAME & ADDRESS *(if different from Controlling Office)* Office of Naval Research Department of the Navy Arlington, Virginia 22217		15. SECURITY CLASS. *(of this report)* UNCLASSIFIED 15a. DECLASSIFICATION/DOWNGRADING SCHEDULE

16. DISTRIBUTION STATEMENT *(of this Report)*

17. DISTRIBUTION STATEMENT *(of the abstract entered in Block 20, if different from Report)*

18. SUPPLEMENTARY NOTES

19. KEY WORDS *(Continue on reverse side if necessary and identify by block number)*

CO Laser	Molecular Kinetics	Energy/Power
Molecular Lasers	Unstable Resonators	Measurements
Electrical Discharge Lasers	Mode Theory	
High Power Lasers	High Efficiency	

20. ABSTRACT *(Continue on reverse side if necessary and identify by block number)*

Effort on the High Power CO Laser Program is reviewed. The program is directed toward the development of the required CO laser technology, the required component technology, and the design and construction of intermediate power laser devices. The results of analytical and experimental investigation of the basic characteristics of the laser and data from a high pressure electrically excited CO laser device are discussed.

DD FORM 1 JAN 73 1473 EDITION OF 1 NOV 65 IS OBSOLETE

UNCLASSIFIED

SECURITY CLASSIFICATION OF THIS PAGE *(When Data Entered)*

2.0 LINE SELECTION (D. K. Rice/P. J. Mendoza)

2.1 Absorption Cell Assembly. Using the information obtained from previous investigations,[1] a large aperture intracavity water vapor absorption cell system was designed and constructed during this period for use in the nominal 10-liter CO EDL. This system will be used to limit the laser oscillations to those spectral lines having high atmospheric transmittance. The details of the absorption cell assembly are illustrated in Figure 2.1. The actual cell is constructed of stainless steel with a high temperature ceramic interior coating. The cell has a 14.0 cm diameter clear aperture and an optical path length of 75.0 cm. The windows are of single crystal calcium fluoride (15Å rms surface roughness, flat to $\lambda/2$ at sodium D wavelength, and a wedge angle of less than 30 seconds of arc). The windows are 15.5 cm in diameter and 1.55 cm thick. The windows are sealed to the cell with silicon rubber O-rings and a stainless steel extension tube to provide a vacuum interface region is attached to each end of the cell. A vacuum seal with the cell is made at one end of the extension tube and a vacuum seal with the laser system at the opposite end. Figure 2.2 illustrates schematically the integration of the absorption cell with the nominal 10-liter CO EDL. The temperature inside the cell is sampled at four places along its length with sealed iron-constantan thermocouples (Gulton Industries Model J20M28) and monitored with a millivolt potentiometer (Leads and Northrup Model 8686).

2.2 Absorption Cell Oven. The absorption cell oven is a forced air oven, capable of reaching and maintaining any temperature between room temperature and 200°C (Bemco Inc. Model F-AMB/400-11.4). The oven contains and also maintains all of the following items at the same temperature: (1) absorption cell assembly, (2) water reservoir, (3) manifold and valves, and (4) pressure transducer. During the use with the nominal 10-liter CO EDL, the absorption cell will be mounted directly to the laser. The oven is supported on a special platform with rubber casters, which makes it portable.

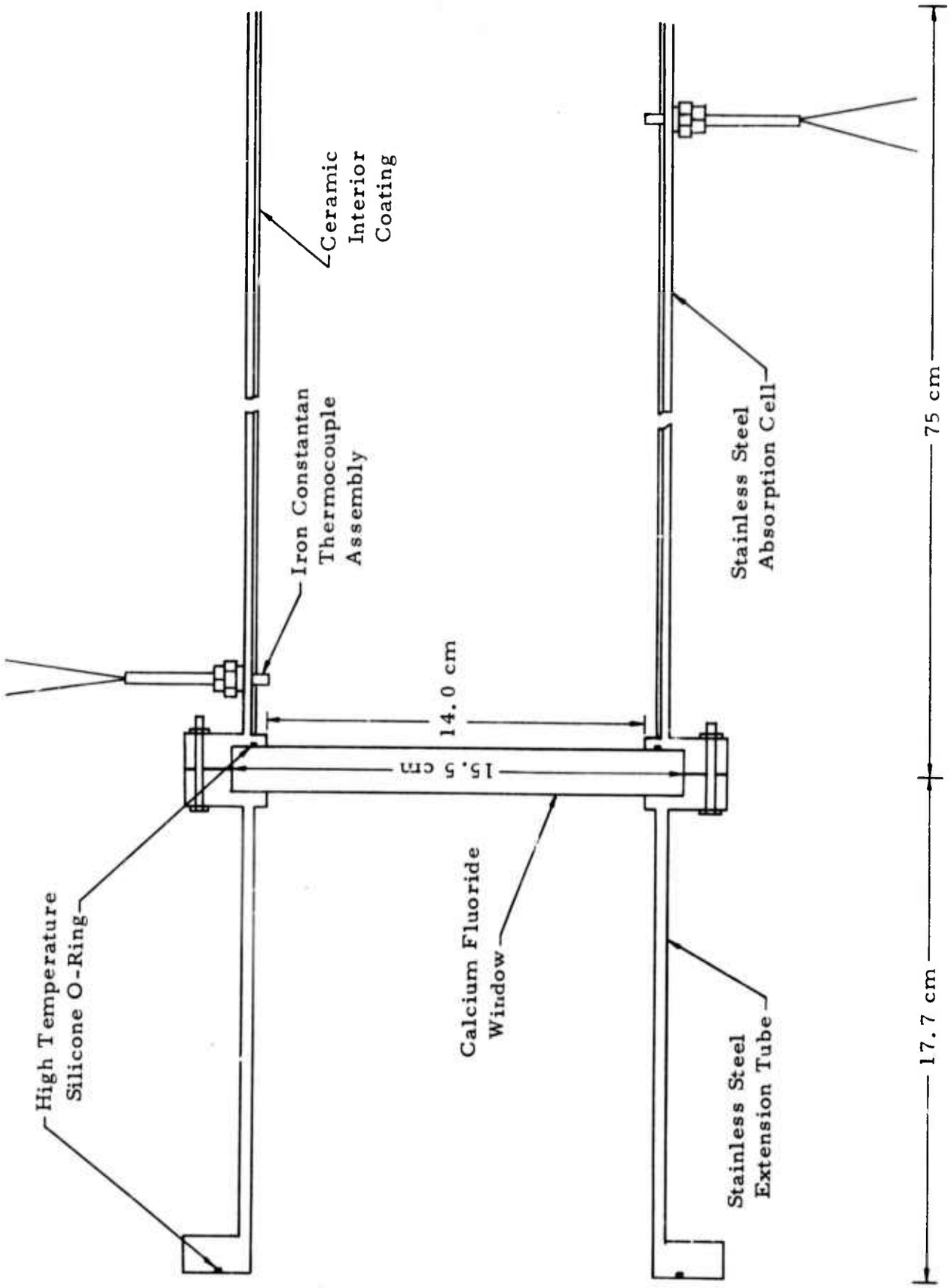

Figure 2.1. Absorption Cell for Nominal 10-Liter CO EDL (Partial Assembly).

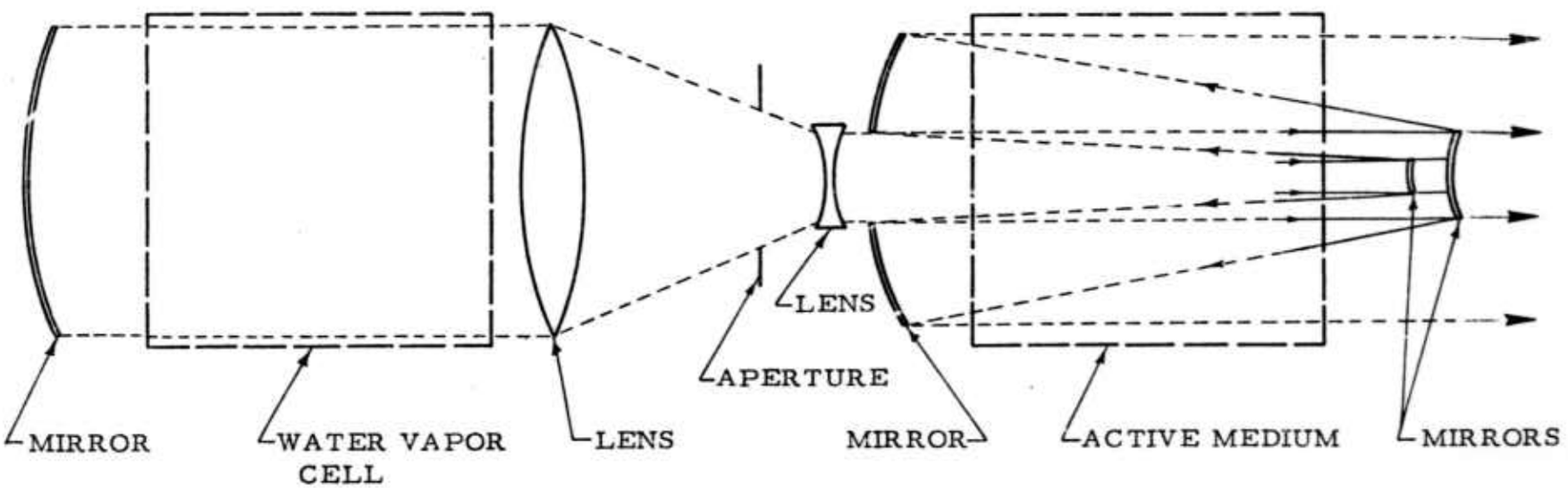

Figure 2.2. Optical Configuration for Line Selected Operation of Nominal 10-Liter CO EDL

2.3 Absorption Cell System. The complete absorption cell system is illustrated in Figure 2.3. All of the tubing inside the oven is stainless steel. All valves are stainless steel bellows type (Nupro Co.). A liquid nitrogen cold trap is installed between the vacuum pump (Welch Model 1402) and the cell to prevent damage to the pump when evacuating water vapor from the cell.

The pressure in the cell was monitored with a high temperature differential pressure transducer (Viatran Model No. 304) in conjunction with a signal conditioner and digital voltmeter (designed and built at Northrop). For cell pressure up to 50 psia, a vacuum pump (Welch Model 1400) is connected to the reference side of the transducer. The vacuum of each of the two Welch pumps is monitored with thermocouple gauges (Consolidated Vacuum Corporation Type GTC-100).

An external line to the manifold provides the capability of adding gases other than water vapor.

2.4 Calibration and Testing of Absorption Cell System. For the testing and calibration of the absorption cell system as an integral unit, pyrex windows were initially installed in lieu of the calcium fluoride windows shown in Figure 2.1. During this phase the high temperature differential pressure transducer (Viatran Model No. 304) was a major problem. The pressure transducer exhibited thermal failure on four separate occasions. On each occasion it had to be removed and returned to the vendor for repair. The manufacturer resolved the pressure transducer problem.

Following calibration and checkout of the absorption cell system, the calcium fluoride windows were installed. The vacuum integrity of the entire system is excellent. The system has a vacuum leak rate of approximately 35 microns per hour.

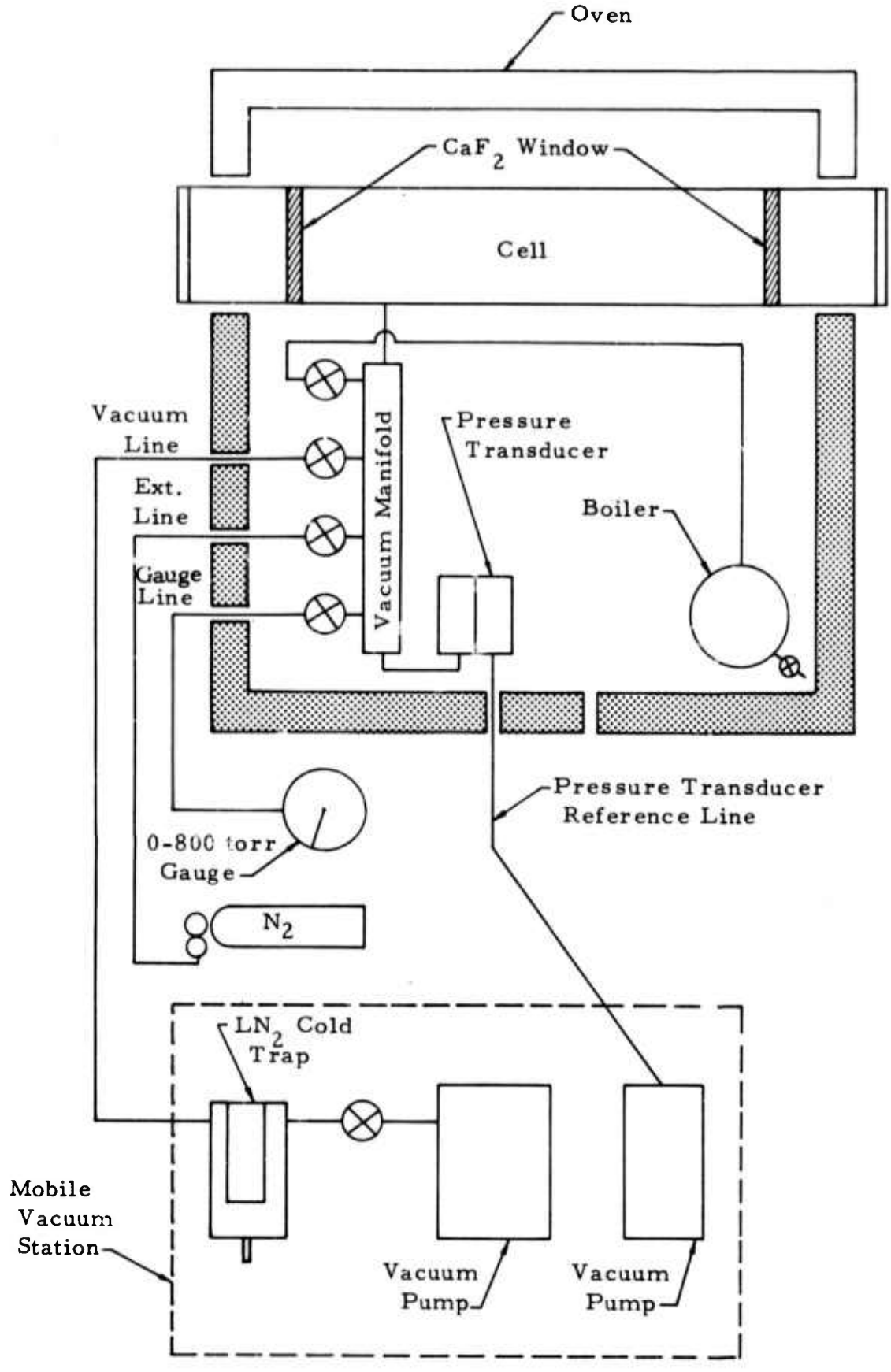

Figure 2.3. Schematic of Absorption Cell System for Nominal 10-Liter CO EDL.

For the remainder of the testing and calibration the pyrex windows were sealed to the end of the stainless steel extension tube shown in Figure 2.1 with silicon rubber O-rings. These windows and the stainless steel extension tube provide a vacuum interface region for the calcium fluoride windows similar to the conditions that exist when used with the nominal 10-liter CO EDL.

The pressure transducer monitoring system was calibrated against two accurate pressure gauges (Wallace and Tiernan 0-800 torr and Wallace and Tiernan 0-100 psi). Dry nitrogen was used for the pressure calibration. Calibration curves were determined at the various operating temperatures.

As stated previously, the temperature inside the cell was sampled at four places. There is a temperature difference of approximately $5^{o}C$ between the end of the cell and the middle of the cell when operating at temperatures over $100^{o}C$.

2.5 Optical Quality Investigations. The nominal 10-liter CO EDL is required to operate as a line selected near-diffraction limited laser and since the absorption cell will be in the optical cavity of the laser, it was necessary to investigate the effect the absorption cell will have on near-diffraction limited operation. Passive interferometry was performed on the absorption cell in order to investigate the optical quality of the cell.

2.5.1 Interferometer Setup. The details of the interferometer are illustrated in Figure 2.4. The absorption cell was placed in the optical path of one of the two equidistant legs of a Mach-Zehnder configuration. Vibrational instabilities in the interferometer limited the resolution accuracy to $\lambda/2$

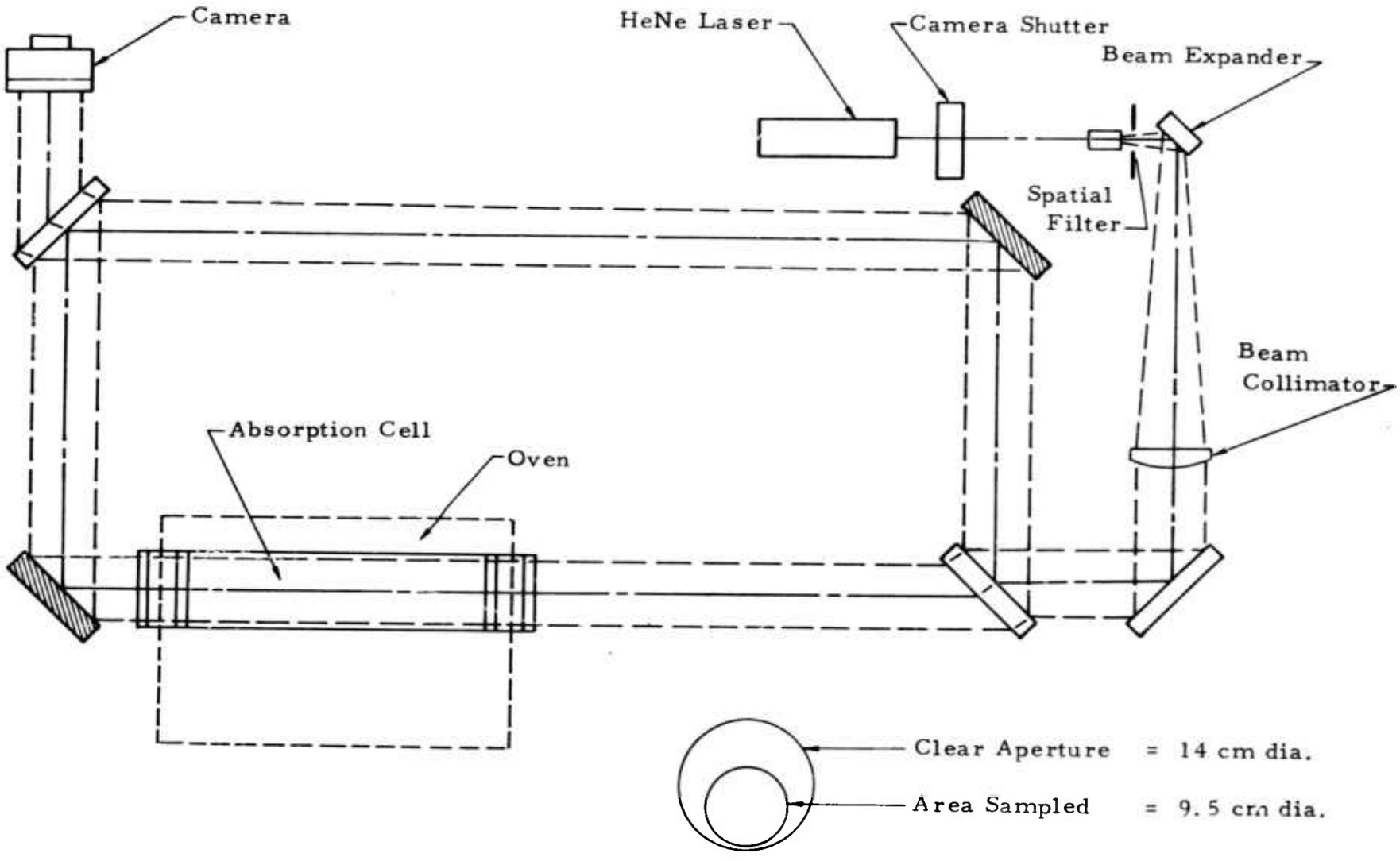

Figure 2.4. Optical Diagnostic Setup for Interferometric Evaluation of Water Vapor Cell for Use in Spectral Line Selection of Nominal 10-Liter CO EDL.

@ 6328Å. The vibrational instabilities were due to the fact that two of the optical elements were mounted on a separate optical bench from the remaining interferometer components.

2.5.2 Pressure Effects on the Optical Quality of the Cell. Figure 2.5 illustrates the basic reference interferogram of the absorption cell at ambient conditions. The irregular fringes in the interferogram are due to the pyrex windows at the end of the stainless steel extension tube. This fringe irregularity is illustrated in the interferogram of the two pyrex windows alone in Figure 2.6. Figure 2.7 illustrates an interferogram of the absorption cell assembly without the pyrex windows at ambient conditions.

The effect of a uniform pressure differential of up to 3 atmospheres across the faces of the calcium fluoride windows was investigated and it was found to have negligible effect on the optical quality of the cell. The absorption cell was pressurized to 3 atmospheres of dry nitrogen at ambient temperature with the end sections evacuated. The interferogram representing these conditions is illustrated in Figure 2.8.

2.5.3 Temperature Effects on the Optical Quality of the Cell. The effect of various temperatures, up to 175°C, on the calcium fluoride windows was investigated and found to have negligible effect on the optical quality of the cell. The absorption cell was evacuated with no pressure differential across the calcium fluoride windows. The cell was heated from ambient temperature to 175°C over a 2 hour period. Figure 2.9 illustrates the interferogram representing the optical effect of 175°C on the absorption cell.

2.5.4 Water Vapor Effects on the Optical Quality of the Cell. The effect of water vapor in the absorption cell caused some observable variations in the optical quality of the cell. It was difficult to discern between thermal effects within the cell from thermal effects outside the cell. The warm end flanges that extend outside the oven had some thermal effects on the air in the optical

Figure 2.5. Reference Interferogram of Absorption Cell for Nominal 10-Liter CO EDL. Cell Conditions are at Ambient.

Figure 2.6. Interferogram of Two Pyrex End Windows Used in Testing Absorption Cell for Nominal 10-Liter CO EDL.

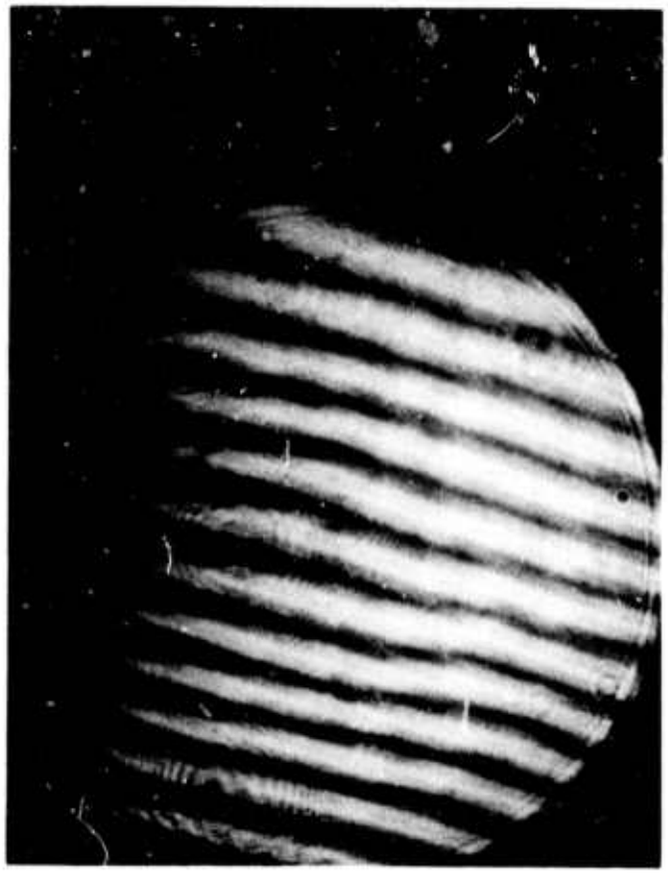

Figure 2.7. Interferogram of Absorption Cell for Nominal 10-Liter CO EDL without Pyrex End Windows. Cell Conditions at Ambient.

Figure 2.8. Interferogram of Absorption Cell for Nominal 10-Liter CO EDL. Cell Conditions: T = Ambient; Pressure of Cell = 3 atm of N_2; End Sections Evacuated.

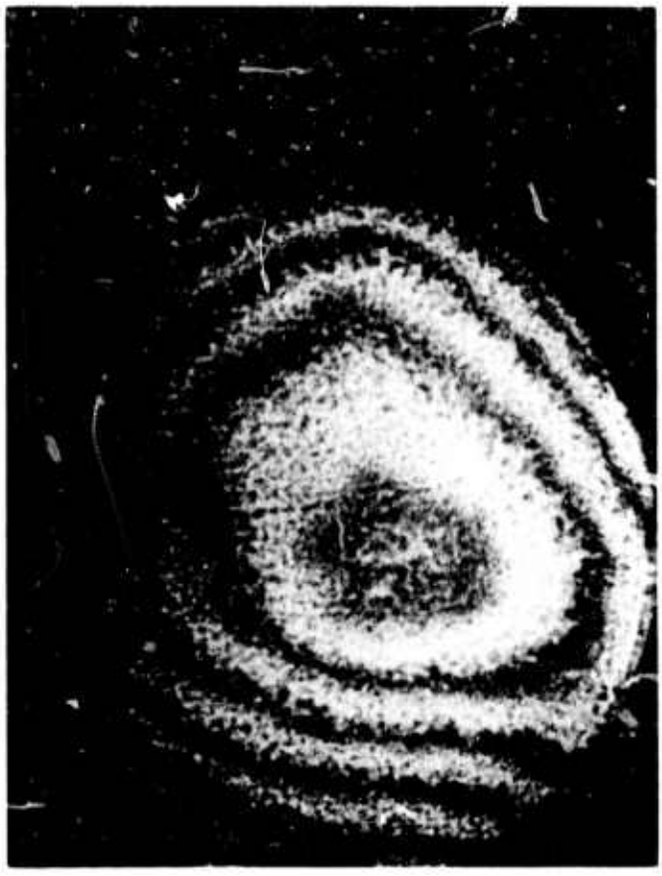

Figure 2.9. Interferogram of Absorption Cell for Nominal 10-Liter CO EDL. Cell Conditions: T = 175°C, Cell and End Sections Evacuated.

path of the interferometer. One thermal variation that could be attributed directly to the water vapor within the cell was in the nature of thermal risers.

The thermal risers moved from the bottom to the top of the cell. It was difficult to quantify and photograph the thermal variations in the fringe pattern since they occurred randomly, lasting in the order of a second. An estimate of the optical variations as a function of thermal variations was made by observing the dynamic fringe pattern variations. The estimate of the optical variations is λ to $\lambda/2$ @ 6328Å. Figure 2.10 shows an interferogram representing the optical effect of 175°C and a water vapor content of 3 atmospheres. The thermal risers were worse at 3 atmospheres than at 2 atmosphere and worse at 2 atmospheres than at 1 atmosphere.

Thermal variations in the fringes were easily discernable from variations due to vibrational instabilities. The vibrational effects were fast compared to the thermal effects.

No vapor condensation occurred on the calcium fluoride windows at any time during this investigation.

The only significant observable anomalies were the thermal riser. Through qualitative observation of their dynamic temporal and spatial characteristics, it was concluded that these risers should have no effect on diffraction limited operation when interfaced with the nominal 10-liter CO EDL.

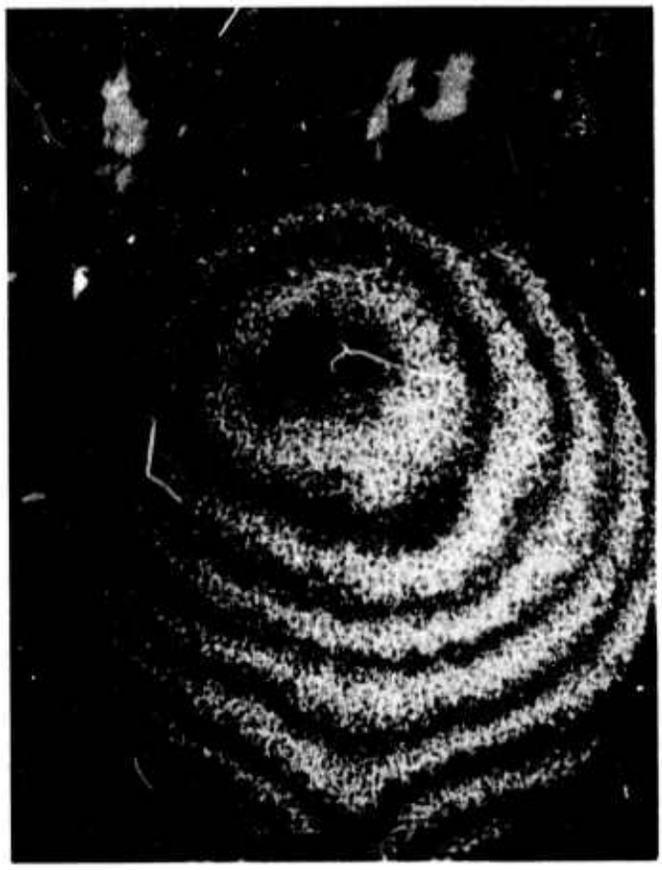

Figure 2.10. Interferogram of Absorption Cell for Nominal 10-Liter CO EDL. Cell Conditions: T = 175°C; Pressure of Cell = 3 atm of H_2O Vapor; End Sections Evacuated.

3.0 A NOMINAL 10-LITER LASER SYSTEM - (W. B. Lacina/G. L. McAllister)

During this reporting period, investigations with the 10-liter device have included experimental investigations of CO/Ar gas mixtures, experimental measurements of the effects of electron beam scattering and interferometric measurements of the cryogenic laser medium with and without electrical excitation.

3.1 Experimental Investigations with CO/Argon Gas Mixtures.

Extensive analyses using the CO kinetics code developed at NRTC[2] have led to scaling generalizations[3] for a pulsed CO EDL applicable over a wide range of parameters including variations in gas pressures, gas mixtures and electrical pumping rates. It is concluded from these scaling generalizations that laser threshold is typically reached after ~0.6 - 1.0J/ℓ-torr of electrical excitation has been deposited in the gas and that steady state operation is obtained after ~1.9 - 2.6 J/ℓ-torr has been deposited. In CO the dominant pumping mechanisms are direct electron excitation into the lower vibrational bands and V-V anharmonic pumping processes. These scaling factors occur because the electrical excitation rate per CO molecule is balanced with the V-V rates which are proportional to the CO partial pressure.

Since VT rates for monatomic diluents are typically very slow, these processes are negligible (to a good approximation) in the kinetics oscillator analysis; their main contributions are secondary electron generation, gain broadening, and gas heating. Hence the scaling laws derived and discussed above depend only upon CO partial pressure, and not total pressure.

Laser threshold times were measured for a range of excitation energies for a 5:1 (Ar/CO) mixture with total pressures ranging from 75 torr to 140 torr. The results are plotted in Figure 3.1 and, as expected, decrease

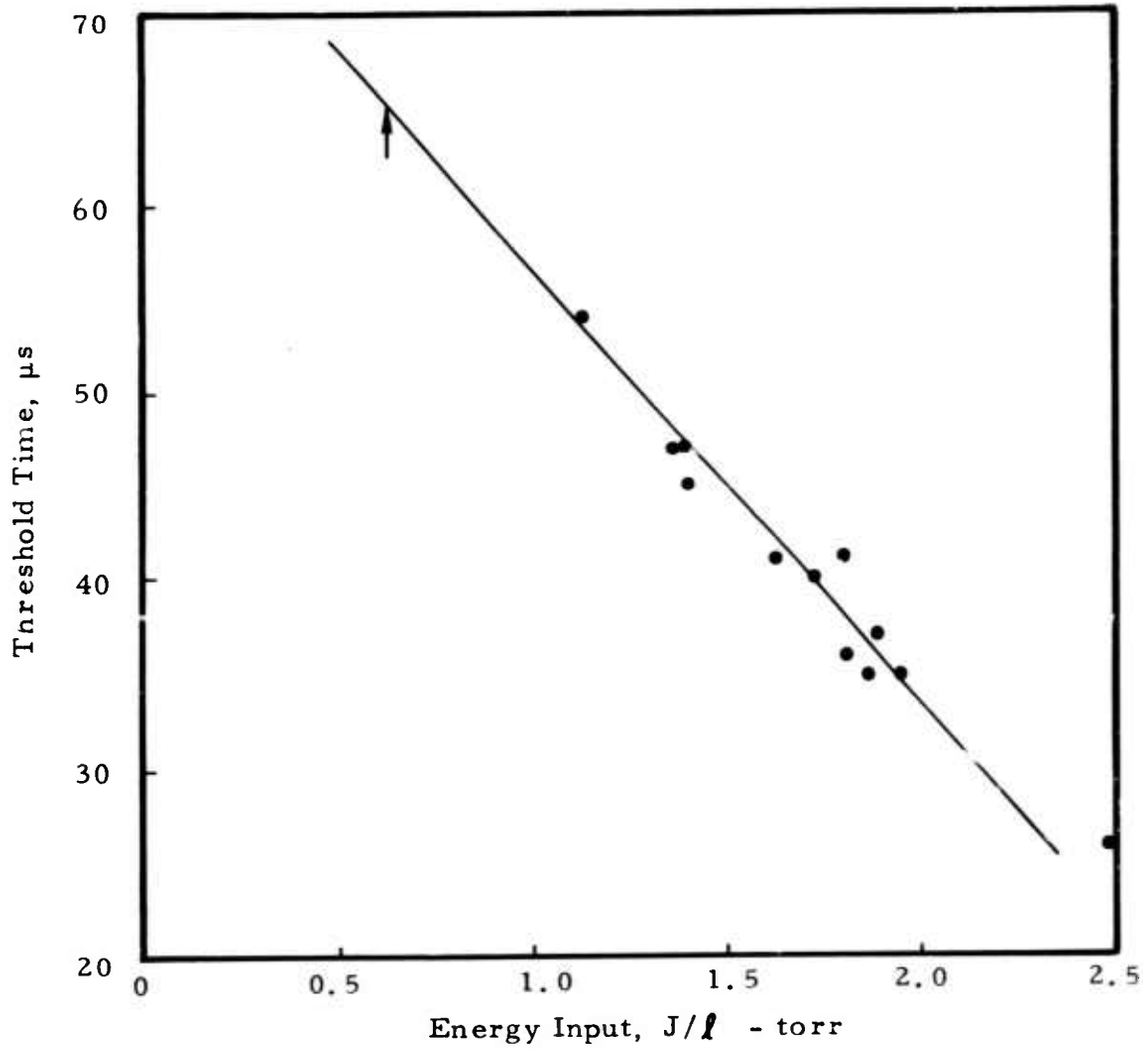

Figure 3.1. Dependence of Threshold on the Excitation Rate.

monotonically as the excitation energy is increased. For these cases, the electrical excitation was terminated at 65 μs and if the data is extrapolated to that point it is found that the threshold excitation is ~0.6 J/ℓ-torr, in good agreement with the scaling generalizations.

Many of the lower excitation rates investigated were insufficient to reach the steady state condition based on the temporal laser intensity profile. Four typical cases where steady state was reached are listed in Table 3.1.

Table 3.1. Steady State Excitation Energy

P_{CO}	P_{Ar}	Sustainer Voltage	Steady State Energy
17 torr	83 torr	4.0 kV	1.88 J/ℓ - torr
17	83	4.0	1.88
17	83	4.5	2.50
20	100	4.5	1.82

The average for these four cases is approximately 2.0 J/ℓ - torr, again in good agreement with the scaling generalizations.

No attempt was made to extend these investigations to higher pressures. Scattering of the primary E-beam current at higher gas pressures becomes significant, leading to nonuniform excitation rates. Therefore, the experimental results would not be expected to match the theoretical results based on an average excitation rate. This problem is discussed further in the following sections with experimental observation of the nonuniform pumping as evidenced by the near-field intensity profiles.

3.2 Effects of Electron Beam Scattering. Prior to entering the discharge region the primary electron beam passes through a 1 mil titanium foil and approximately 2 cm of cryogenic gas. For typical primary voltages

(<200 kV) and typical pressures (≥100 torr) of cryogenic (80°K) gases, the scattering can be severe with many electrons lost to the discharge wall. This leads to nonuniform excitation, particularly in the vertical direction from cathode to anode, and affects the energy extraction and mode pattern. This problem can be reduced by increasing the discharge region width and/or by decreasing the cathode-anode separation. However, even in the present square configuration the problem is significant.

Near-field burn patterns of the laser output with CO/Ar mixtures were studied for a range of gas pressures and primary electron voltages to illustrate these effects. Figure 3.2 illustrates three near-field patterns for 150 torr of CO/Ar (5:1) at 80°K with an excitation rate of approximately 2.5 J/ℓ - torr. The E-gun voltages are, from top to bottom, 175 kV, 165 kV and 155 kV. Empirical correlation of experimental results has shown the scatter distribution for a pencil beam of electrons passing through a thin scatterer, in which the electron energy loss is much less than the initial electron energy, can be accurately described by a Gaussian distribution function[4]

$$f(\theta) = \frac{1}{\sqrt{2\pi}\theta} \exp(-\theta^2/2\bar{\theta}^2) \qquad (1)$$

where $\bar{\theta}$, the mean scatter angle, is a function of both the primary electron energy and the area density of electrons in the scatter.

A convenient correlation[5] from which to obtain values of $\bar{\theta}$ and one which agrees well with experiment is

$$\bar{\theta} = 56.6^{\circ}(d/R_o)^{1/3} \qquad (2)$$

where d is the scatterer thickness in mg/cm^2 and R_o is the electron range in the medium in mg/cm^2. The scattering dependence on the

voltage enters only through the range, R_o, and is therefore reasonably insensitive to small changes; however, the degradation in the pattern at 155 kV [Figure 3.2 (a)] is obvious. As the voltage is reduced the scattering becomes worse, reducing the relative electron density near the anode (bottom) which in turn increases the resistivity and the excitation rate in that region. As evidenced by Figure 3.2 the laser emission near the cathode (top) is thereby reduced.

The computer code developed by Olson[6] was used to estimate the effects of electron scattering for three different total gas pressures and the results are plotted in Figure 3.3. It is asumed here that the gas conductivity is proportional to the square root of the primary beam current[7] and the electric field is calculated, normalized to the case for no scattering. The conditions were the same as those above except the E-gun voltage was held constant at 175 kV and the pressure was varied from from 300 torr to 75 torr. As expected the scattering effects are very obvious in this case and the near-field burn patterns show this. Near-field patterns are shown for these cases in Figure 3.4. The improvement at lower pressures is obvious and, in fact, the pattern at 75 torr [Figure 3.4 (c)] looks like the pattern expected from this optical configuration which was a confocal unstable resonator with a truncated circular aperture.

The normalized electric fields, plotted in Figure 3.3 for 300 torr and 75 torr were used and a uniform current assumed to compute an electrical pumping distribution for conditions simulating those of Figure 3.3 (~2.5 J/ℓ - torr). The theoretical scaling generalizations given by Lacina[3] were then used to estimate the overall efficiency for each excitation rate. Finally this efficiency was multiplied by the excitation rate to compute the extracted energy density as a function of position. These calculations are

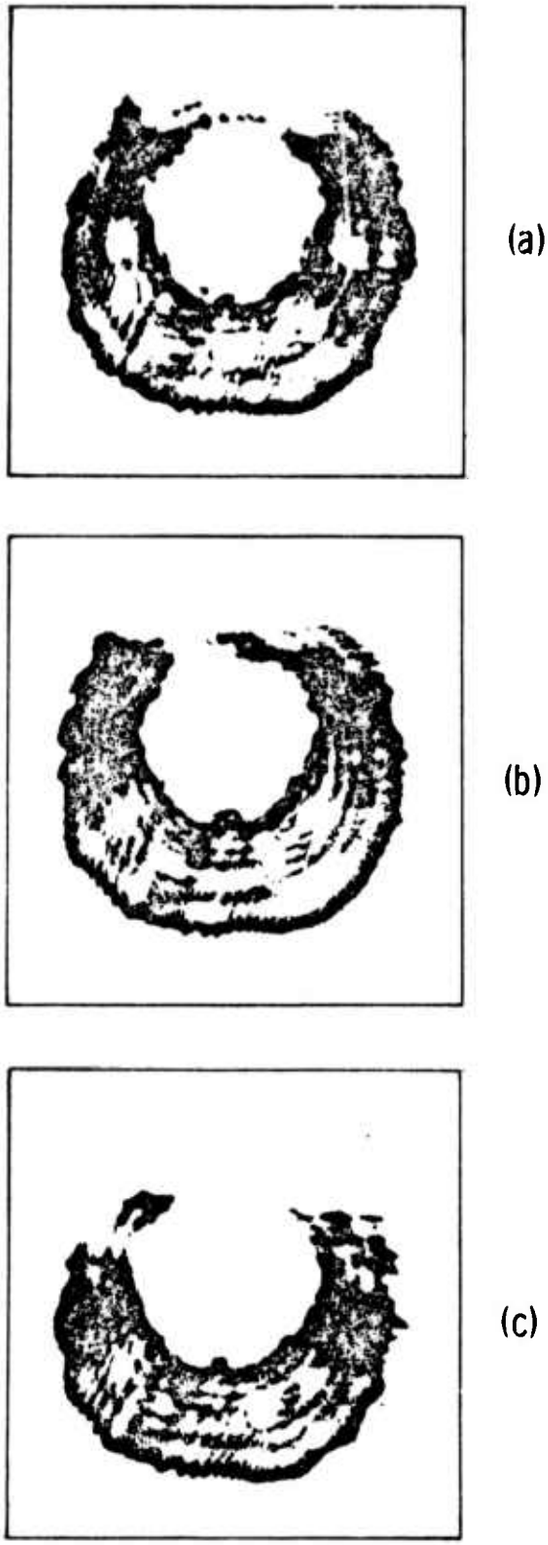

Figure 3.2. Near Field Burn Patterns for E-Beam Voltages of (a) 175 kV, (b) 165 kV and (c) 155 kV.

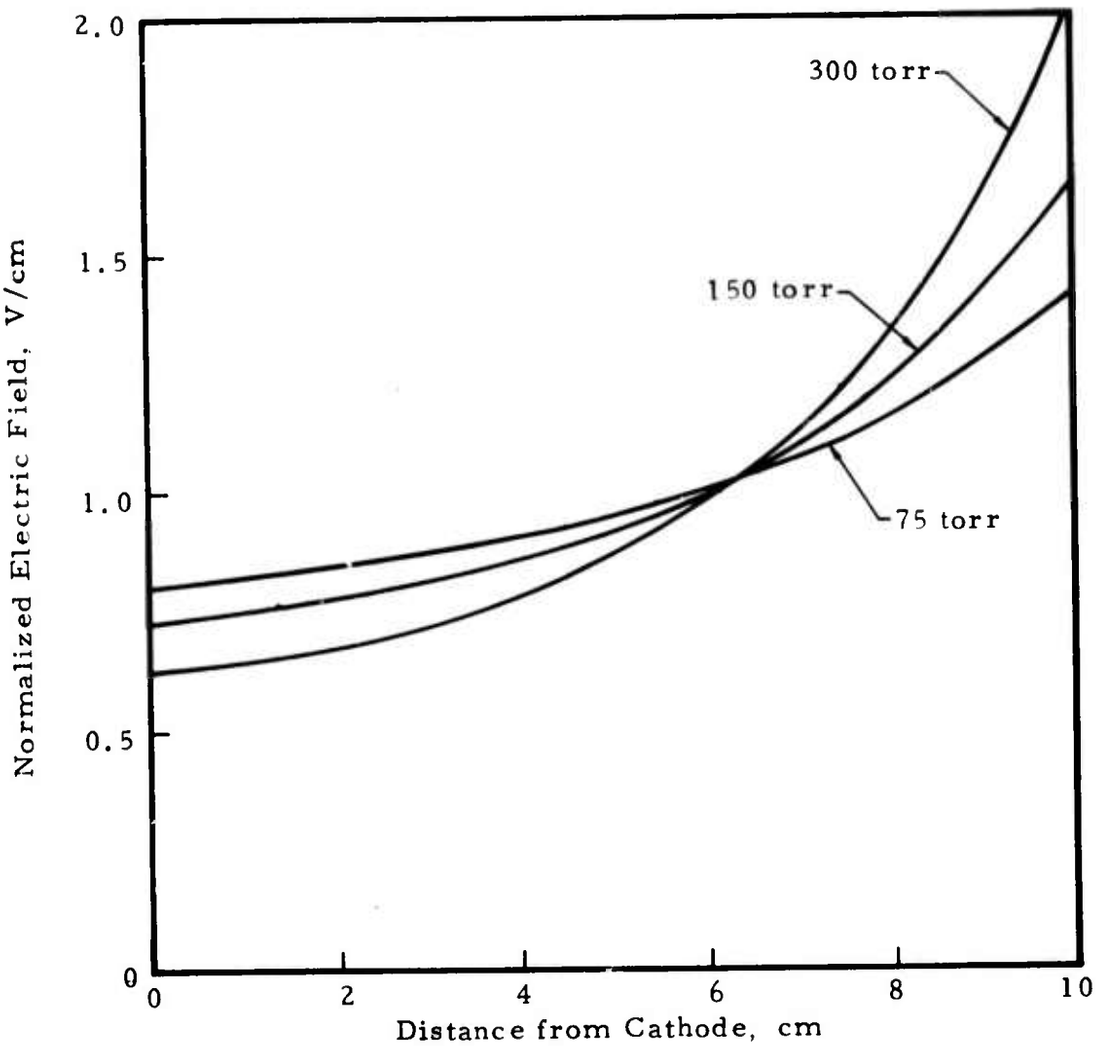

Figure 3.3. Normalized Electric Field Intensity as a Function of Distance from Cathode.

Figure 3.4. Near Field Burn Patterns for an Ar/CO (5:1) Mixture at (a) 150 torr, (b) 100 torr and (c) 75 torr.

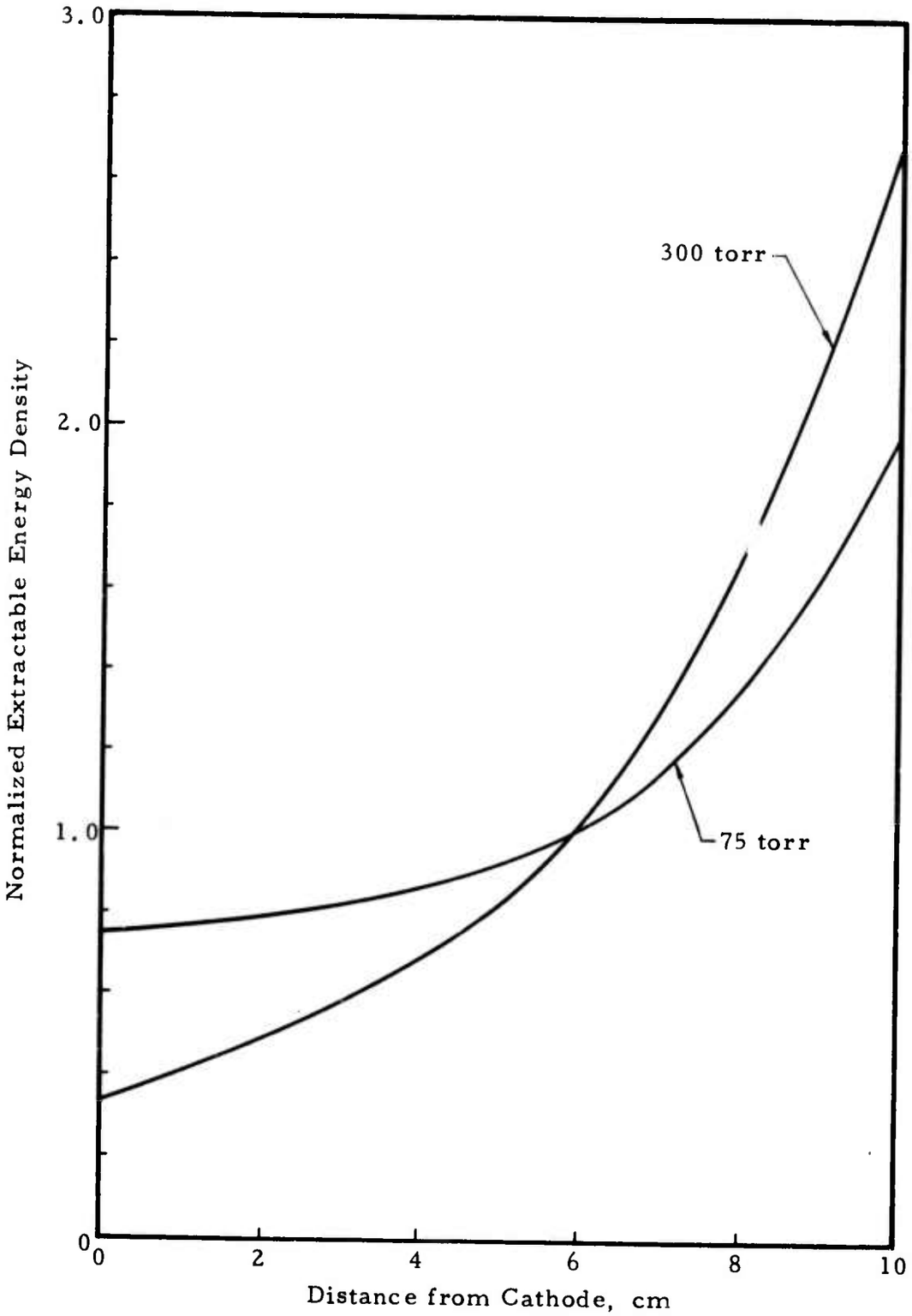

Figure 3.5. Normalized Extractable Energy Density as a Function of Position.

plotted in Figure 3.5, normalized to the theoretical energy density extracted with the average electric field intensity. Again the degradation in uniformity is obvious at the higher pressures.

The problems associated with electron scattering are clear from the above results and operation at higher pressures using argon as a diluent is not expected to produce good results unless higher E-beam voltages or oversquare discharge regions are used.

3.3 Laser Medium Interferometry. A Mach-Zehnder interferometer utilizing a ruby laser source was used to study the cryogenic laser medium with and without electrical excitation. The experimental configuration is illustrated in 3.6. The interferometer was normally adjusted to have several fringes per centimeter, aligned vertically. This spacing is convenient for both single and double pulse interferograms in that they are spread far enough to easily follow the individual fringe paths yet are spaced closely enough to observe Moire' patterns when double pulse interferograms are taken. The fringes were aligned vertically because the dominant acoustic waves are from the anode and cathode hence the fringes were approximately normal to the disturbances and more easily interpreted.

In all of the interferograms the laser aperture (a truncated circle) is somewhat larger, even after reducing the size, than the camera aperture. For clarity a mask is overlaid on the interferograms indicating the true shape of the CO laser discharge aperture. For reference, the true diameter of the limiting circle is 9.25 cm. The ruby laser is described in the first section below followed by a description of the interferometry results.

3.3.1 Ruby Laser Description. The Northrop constructed ruby laser was operated in the Q-switched mode with a typical output of 10 mJ in

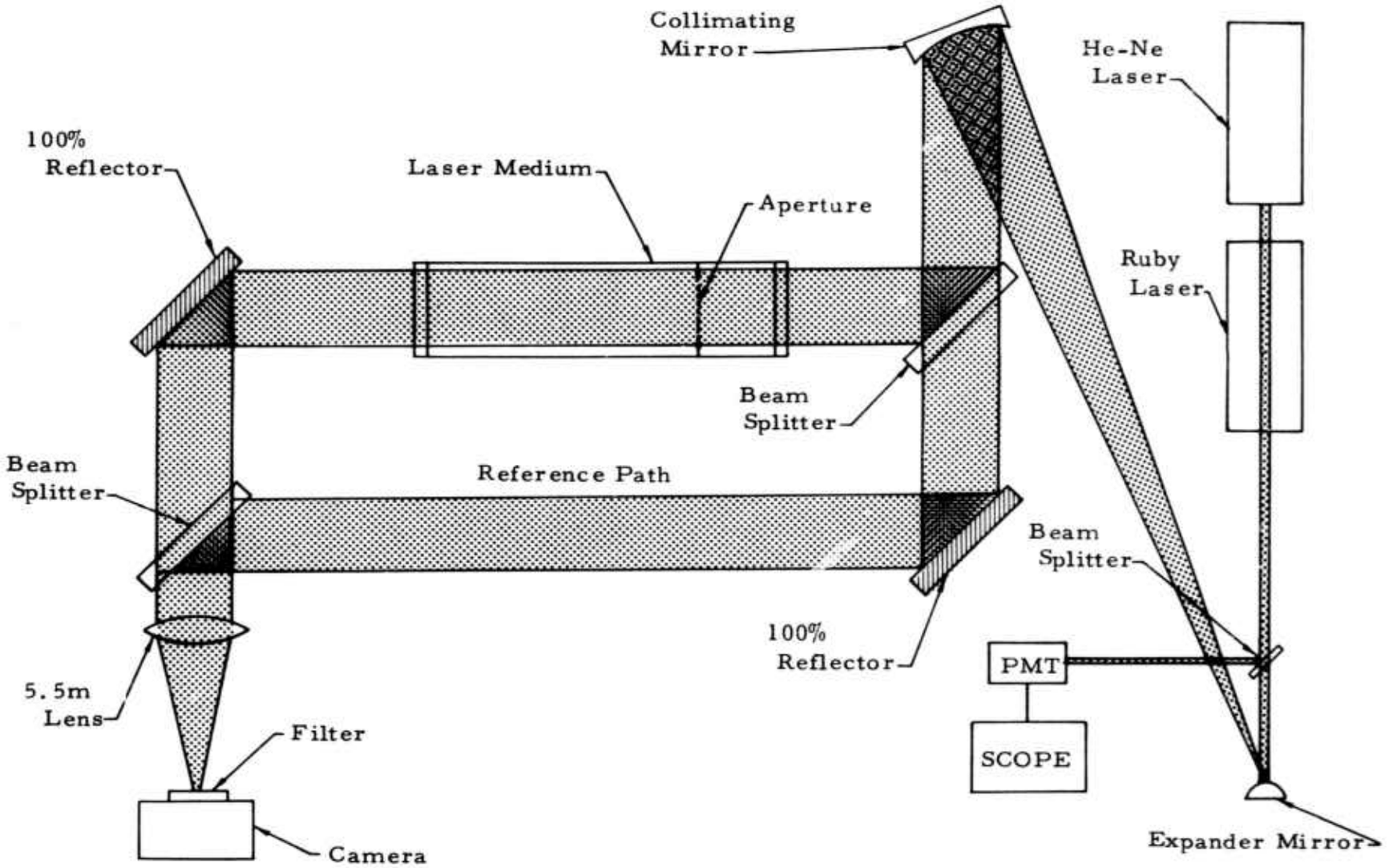

Figure 3.6. Interferometer Configuration for Acoustic Studies.

approximately 20 ns. Temperature control is maintained by passing liquid nitrogen boiloff through a valve controlled by a thermocouple mounted inside the laser head. The cavity is a double elliptical reflector with two excitation linear flash lamps driven by a square-wave pulse from an LC network storage bank. Transverse mode selection is obtained by aperturing the capacity to reduce the Fresnel number ($N \approx 2$) while the number of longitudinal modes emitted depends upon the Q-switching techniques used and the timing accuracy desired.

Optimum timing accuracy was obtained by Q-switching with a Pockel's cell. Double-pulse interferograms were possible in this configuration with precise control on the pulse separation. However, very little longitudinal mode control is obtained with the Pockel's cell and the slight imbalance in path lengths was sufficient to make the fringe visibility poor. Additional longitudinal mode selection was obtained by adding a weak passive Q-switch dye solution (cryptocyanine dissolved in methanol) in series with the Pockel's cell. The timing capability is thus retained and the fringe visibility is improved. A typical result is illustrated in Figure 3.7 (a). For single pulse interferograms where the timing accuracy requirements are ≥ 10 μs the passive Q-switch solutions can be used exclusively. This results in single mode operation and excellent fringe visibility as illustrated in Figure 3.7 (b), even with unbalanced path lengths. The majority of the studies described below are single-pulse interferograms of the acoustical waves and used the last configuration for optimum fringe visibility.

3.3.2 Interferometry of the Passive Laser Medium. Temperature conditioning problems are extreme for the CO laser because of the cryogenic gas temperatures required and the high pressures of operation. The gas conditioning system in present use has been described in detail in previous reports and consists of a large roughing heat exchanger to bring the gas down

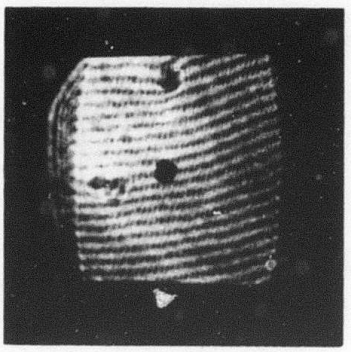

(a)

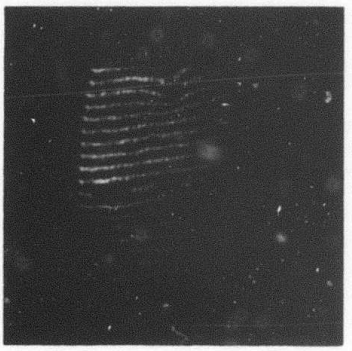

(b)

Figure 3.7. Interferograms Taken with Ruby Switched by (a) Pockel's Cell Plus Passive Dye Cell and (b) Passive Dye Cell Only.

near liquid nitrogen temperature followed by a final heat exchanger which also serves as the sustainer anode. The prepared gas flows vertically upward through the porous anode and is extracted above the porous cathode. The discharge sidewalls are liquid nitrogen cooled and the gas is thus surrounded, except at the top, by a liquid nitrogen jacket.

The temperature stability of the passive gas system is illustrated by the double-pulse interferograms shown in Figure 3.8. The conditions for this interferogram were 100 torr of pure nitrogen at 80°K with 8 grams per second flow rate. Figure 3.8 (a) is a double pulse interferogram with 50μs between pulses. As expected, no change occurs in the gas flow during this period; hence the fringes are exactly overlapping and the interferogram looks like a single pulse interferogram. In Figure 3.8 (b) the pulse separation is approximately two minutes which is long compared to the period for either motion in the interferometer or changes in the gas density. In this case the two fringe patters are displaced and the resulting Moire' pattern indicates that the change in the optical path length is 3 fringes (3λ at 6943 Å) across the medium. This amounts to a total difference in optical path length of less than one half wavelength at 5μ and includes the stability of the interferometer which has approximately 8 meter arms and includes 2 separated tables. Nitrogen/CO gas mixtures and Ar/CO mixtures have also been studied and appear similar.

3.3.3 Interferometry of the Active Medium. When the laser discharge is excited acoustical perturbations are produced because of the intense heating in the cathode fall region and because of the bulk heating of the medium. These give rise to acoustical waves moving into the medium from the top (cathode) and the bottom (anode). The magnitude of the disturbance and the velocity of propagation depend on the amount of gas heating.

Figure 3.8. Double Pulse Interferograms of Passive Cryogenic Laser Gas with Pulses Spaced by (a) 50 μs and (b) 2 Minutes.

Parametric measurements have been made for N_2, CO/N_2 and CO/Ar gas mixtures under electrical excitation without optical extraction. For each a range of excitation rates were studied. These rates were controlled independently in current and voltage by varying the sustainer voltage and the primary E-beam current. Typical data is shown in Figure 3.9 for 100 torr of nitrogen. In Figure 3.9 (a) the excitation rate is 135 W/cm^3, in (b) it is 400 W/cm^3 and in (c) 1250 W/cm^3. The ruby pulse occurred 180 μs after initiation of the 80μs laser discharge and as is evident from the photographs there are three distinct disturbances. An anode wave is propagating vertically upwards due to bulk heating of the gas causing an expansion of gas out of the cavity into the porous anode. A similar wave occurs at the top and, in addition, a third wave occurs due to the more intense heating in the cathode fall region localized near the cathode. This gives rise to a sharp density gradient propagating downward which is observed as a sharp break in the fringes and also gives rise to an expansion wave propagating in both directions from the cathode. The increase in the intensity of the disturbances and the velocity of propagation can be clearly seen by comparing the three photographs in Figure 3.9.

This data is presently being analyzed to estimate the magnitude of the cathode wave and the bulk heating rate and the results will be reported next quarter.

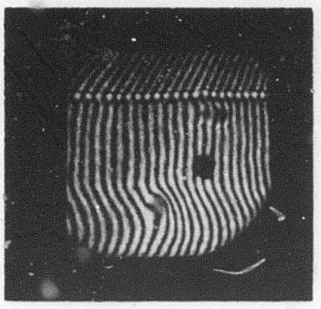

(a)

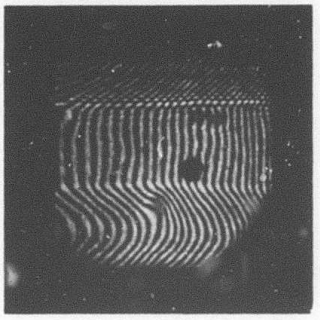

(b)

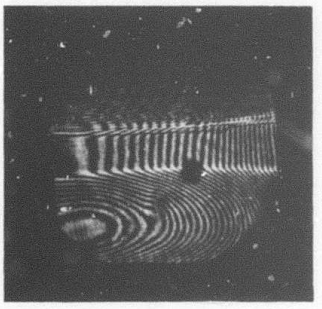

(c)

Figure 3.9. Interferograms for Electrically Excited Laser Gas Pumped at (a) 135 W/cm^3, (b) 400 W/cm^3 and (c) 1250 W/cm^3.

REFERENCES

1. Northrop Report NLSD 72-7R, "Semi Annual Technical Status Report, High Power CO Laser," March 1972.

   D. K. Rice, "Absorption Measurements of Carbon Monoxide Laser Radiation by Water Vapor," AD 746-170 (July 1972).

   D. K. Rice, "Carbon Monoxide Spectral Line Selection Studies," AD 749-823 (August 1972).

   Northrop Report NRTC 72-10R, Fourth Quarterly Technical Status Report, High Power CO Laser," September 1972.

   D. K. Rice, "Absorption Measurements of Carbon Monoxide Laser Radiation by Water Vapor," presented at Autumn Meeting of Optical Society Association, 17-20 October 1972, San Francisco, California.

   D. K. Rice, "Absorption Measurements of Carbon Monoxide Laser Radiation by Water Vapor, Appl. Opt., Vol. 12, No. 2, pp 218-225 (February 1973).

   D. K. Rice, G. L. McAllister, R. G. Eguchi, and M. M. Mann, "High Efficiency Operation and Spectral Line Selection of a High Pressure CO Laser," Paper 11-A presented at 1973 IEEE/OSA Conference on Laser Engineering and Applications (Washington, D.C.), 30 May - 1 June 1973.

   Northrop Report NRTC 73-38R, "Sixth Quarterly and Semiannual Report, High Power CO Laser," November 1973.

2. W. B. Lacina, M. M. Mann, and G. L. McAllister, "Transient Oscillator Analysis of a High Pressure Electrically Excited CO Laser," IEEE Journal Quant. Elect. QE-9, 588 (1975).

   W. B. Lacina, "Kinetic Model and Theoretical Calculations for Steady State Analysis of an Electrically Excited CO Laser Amplifier System," Northrop Report NCL 71-32R, August 1971.

3. Northrop Report, NRTC 73-43R, Scaling Generalizations for a Pulsed CO EDL, W. B. Lacina, October 1973.

4. R. E. Center, "Plural and Multiple Scattering of Fast Electrons in Gases," Phys. Fluids 13, 79 (1970).

5. V. F. Baranov and O. A. Pavlovskii, "Passage of Electrons through Matter," Atomnaya Energiya 25, 317 (1968).

6. N. T. Olson, Northrop Research and Technology Center, private communication.

7. B. B. O'Brien, Jr., "Electron Density in an Electron Beam Stabilized High Pressure Discharge," Northrop Report NLSD 72-8R, March 1972.